Control Engineering Practice 91 (2019) 104107

Contents lists available at ScienceDirect

Control Engineering Practice

journal homepage: www.elsevier.com/locate/conengprac

Optimal operation of oil and gas production using simple feedback control structures

Dinesh Krishnamoorthy [a,b,*], Kjetil Fjalestad [b], Sigurd Skogestad [a]

[a] Department of Chemical Engineering, Norwegian University of Science and Technology (NTNU), Trondheim, Norway
[b] Equinor Research and Technology Center, Porsgrunn, Norway

ARTICLE INFO

Keywords:
PID control
Automation
Oil and gas production
Optimal control
Feedback-based optimization

ABSTRACT

The purpose of this paper is to describe the control challenges related to optimal operation of oil and gas production wells, and show that optimal operation can be achieved using simple feedback control structures. In particular, we find that conventional feedback control structures can efficiently handle changes in active constraint regions using simple logics such as split-range and selectors. This eliminates the need for complex models to be used in the optimization problem, and in addition eliminates the need to solve numerical optimization problems online. Thus, by using only simple feedback controllers that have been used widely in the oil and gas industry, it has a higher chance of implementation. We demonstrate the use of simple feedback controllers on two application examples; 1) a gas-lift optimization simulation study with a network of six gas-lifted wells, 2) an experimental study of optimal control of electrical submersible pump (ESP) lifted oil wells tested on a large-scale experimental test facility with a full scale ESP and live viscous crude oil.

1. Introduction & motivation

The operation of an oil and gas production unit involves making various decisions which affects the production volume and the cost of production. Typically these decisions are taken at different time scales to meet the short-, medium- and long-term objectives. The long term decisions typically involve selecting drilling schedules, and production and injection strategies that affect the reservoir drainage over the entire life time of the field. This is typically known as reservoir management. The medium-term decisions are taken in the time scale of hours to days to maximize the daily operating revenue of the oil and gas production unit. This is known as *daily production optimization*. Typical decisions involve selecting the choke opening of the different wells, allocating shared resources such as available lift gas or power in order to maximize the daily operational profits, and ensure that the process and operating constraints are satisfied. The short-term decisions are made in lower-layer control system and may include short-term corrective actions, for example, to avoid valve saturation or too high pressures on a fast time scale. Finally, there is a safety and automation system (SAS) that accounts for fast corrective actions and triggers safety valves in case of emergencies, but this is generally a completely separate system and outside the scope of this paper. This paper will focus on the daily production optimization problem, which is equivalent to real-time optimization (RTO) from a process systems perspective.

In the face of volatile oil prices, competitive markets and increased focus on sustainable oil and gas production, daily production optimization plays a vital role in maximizing the operational profits and reduce unwanted shut-down, gas flaring, and power consumption. Daily production optimization has been shown to increase production volume by 1%–4% (Palen, Goodwin, et al., 1996), reduce downtime (Hedrick, Philips, Crivello, & Sakoclus, 2003), provide more accurate and optimal allocation (Reeves, Harvey Jr., Smith, et al., 2003), reduce decision-cycle time and reduce operator workload (Mochizuki et al., 2004). All these benefits have also led to the formation of a technical interest group in the Society of Petroleum Engineers (SPE) focusing on real-time optimization for oil and gas production systems, which indicates the importance of the real-time optimization in the upstream oil and gas industry (Bieker, Slupphaug, Johansen, et al., 2007; Mochizuki et al., 2004). Despite this interest, real-time optimization is still not widely used in oil and gas production. There are two main reasons for this, namely, technological limitations and corporate culture, which are briefly discussed below.

1.1. Technological limitations

Traditional real-time optimization requires a detailed mathematical model of the process which is used online to solve a numerical optimization problem. The main technical challenges with this approach are: (in expected order of importance)

1. Lack of good models that represents the system (Offline model development)

* Corresponding author at: Department of Chemical Engineering, Norwegian University of Science and Technology (NTNU), Trondheim, Norway.
E-mail addresses: dinesh.krishnamoorthy@ntnu.no (D. Krishnamoorthy), kfja@equinor.com (K. Fjalestad), skoge@ntnu.no (S. Skogestad).

https://doi.org/10.1016/j.conengprac.2019.104107
Received 2 April 2019; Received in revised form 22 June 2019; Accepted 1 August 2019
Available online 22 August 2019

2. Wrong value of parameters and disturbances used in the model (Online model update)
3. Numerical robustness, including computational issues
4. Inconsistency issues between optimization layer and control layer.

One of the primary bottlenecks of model-based optimization tools is the lack of accurate models (reason 1). Firstly, developing such models require domain expertise, and is very time consuming. Furthermore, with the emergence of new and challenging field and reservoir conditions such as unconventionals and heavy oil fields, existing first-principle models that describes the pressure drop in the wells or reservoir inflow etc. may not be able to accurately represent the real system. Finally, lack of knowledge and/or model simplification makes such optimization tools less relevant.

The model used in the optimization also needs to be updated regularly based on the real-time process measurements. This repeated cycle of *measure–update–optimize* is necessary to ensure that the system is operating optimally when operating conditions vary. However, if steady-state process models are used, it is necessary to wait for the plant to settle to a new steady-state before the model can be updated. If the process is subject to frequent disturbances, or if it takes a long time to settle to steady-state, then the process will be operated sub-optimally for long periods due to the steady-state wait time. As noted by Darby, Nikolaou, Jones, and Nicholson (2011), the steady-state wait time is a fundamental limitation of the traditional RTO approach (reason 2).

One obvious solution to address the steady-state wait time is to use dynamic optimization tools such as dynamic RTO, or the closely related, economic nonlinear model predictive control (ENMPC). However, dynamic optimization problems require high computational capacity, which is challenging even with today's computing power. In a recent paper (Campos, Teixeira, Liporace, & Gomes, 2009), the authors note that several numerical issues need to be addressed before dynamic optimization can be widely used for oil and gas production (reason 3). Moreover, safety requirements in offshore oil and gas production may also require the implementation of automatic tools on rugged embedded platforms such as programmable logic controllers (PLC), which are currently not suited for solving nonlinear optimization problems online (Binder, Kufoalor, Pavlov, & Johansen, 2014). Foss, Knudsen, and Grimstad (2018) also concluded that, static optimization formulations are sufficient for many production optimization problems in the oil and gas industry.

Finally, the optimal solutions computed by the optimization layer is often provided as setpoints to the controllers in the automation layer. It may happen that the setpoints are not be feasible for the lower level controllers (reason 4). This may be due to the unmodeled effects in the optimization layer or due to the multivariable coupling between the different control loops that are not taken into account in the optimization layer. Although there is active research in academia and industry to address these technological challenges, they are far from being the industry standard in oil and gas production.

1.2. Human aspects

In a recent review paper (Mochizuki et al., 2004), the authors very aptly identified "people" and human aspects as one of the major components when addressing challenges related to adopting new technology. These can be broadly divided in two categories,

1. Corporate culture
2. Technical competence

Corporate culture forms the foundation of how an organization works and plays a vital role in adopting a new technology. The corporate culture in some organizations may be such that major changes such as deployment of new technology are resisted. Instead, one prefers "trusted" technology in order to minimize liability (Mochizuki et al., 2004). Operator confidence is another important aspect, as they are the end users. Failure to gain operator confidence will thus lead to an unsuccessful implementation of the technology.

Lack of competence and training is another major issue when adopting advanced optimization tools. As mentioned in Section 1.1, models and optimization tools require regular maintenance and re-tuning in order to sustain the performance improvements. For example, changes in reservoir conditions, instrument degradation and changes in process equipment leads to performance degradation. The expected benefits from using optimization tools such as real-time optimization and model predictive control are at a risk without regular monitoring and maintenance (Forbes, Patwardhan, Hamadah, & Gopaluni, 2015). Since the optimization layer is generally a multivariable and large-scale problem, the complexity and the understanding of the optimization concepts present key challenges for the end users (Mayne, 2015; Qin & Badgwell, 2003). Often, expert knowledge is required to perform the maintenance, which may be limited in the organization. With increasing number of applications, there is a paucity of skilled engineers to provide maintenance and support to sustain the benefits. As noted by Forbes et al. (2015), skilled engineers involved in the initial implementation are often not available for maintenance, resulting in performance degradation and the application being turned off by the operators.

In summary, the limited use of advanced optimization tools in the oil and gas industry is due to the combination of technological challenges and the human aspects. In this paper, the aim is not to provide new algorithms, but instead show how some of these challenges can be circumvented using exisiting tools such as simple feedback controllers. In other words, the objective is to reduce the need for a separate centralized optimization layer, and instead move the optimization objectives into the control layer by using simple logic blocks (Krishnamoorthy & Skogestad, 2019).

Simple feedback controllers like PID controllers have been used in the oil and gas industry for several decades. PID controllers can be easily implemented on the existing process control system without the need for any additional software or hardware infrastructure. More importantly, simple feedback controllers are well-known "trusted" tools that are implemented on a familiar interface to many engineers and operators alike, and hence it eliminates the dependency on skilled engineers to monitor and maintain such tools. Consequently, the operator confidence and corporate culture issues are also circumvented. The use of simple feedback controllers do not require the use of detailed mathematical models online, nor does it require the need to solve numerical optimization problems. By eliminating a separate optimization layer and incorporating the optimization objectives into the control layer, we also avoid the potential feasibility issues between the optimization and control layers.

To this end, we will show that, by using conventional feedback control structures along with simple logic blocks, we surpass most of the technological and people-related challenges described above. In fact, it is not surprising to see the prevalence of simple feedback control structures and logic blocks in many industrial applications. However, these are often developed based on good engineering intuition and best practices. Probably, because these structures were viewed as old-fashioned and to soon be replaced by methods such as MPC, there has been virtually no academic research in this area for about 70 years since these structures were first introduced in the 1940's. Thus, there are almost no systematic tools for designing such structures, until recently with the works of Krishnamoorthy and Skogestad (2019), Reyes-Lúa, Zotică, Das, Krishnamoorthy and Skogestad (2018) and Reyes-Lúa, Zotică and Skogestad (2018).

In this paper, we demonstrate the use of conventional feedback controllers for optimal operation of offshore oil and gas production systems. We first consider a network of gas lifted wells in Section 3. Using a simulation case study, we show that optimal operation can be achieved using simple feedback controllers. In Section 4 we apply this approach for optimal operation of an electric submersible pump (ESP)

lifted well. Using a large scale experimental test facility equipped with a full scale electric submersible pump and live multiphase viscous crude oil, we validate the use of such simple feedback controllers for optimal operation.

2. Preliminaries

2.1. Active constraint control

The idea of systematically translating economic objectives into control objectives dates back to the 80's, where the concept of *feedback optimizing control* was initially proposed by Morari, Arkun, and Stephanopoulos (1980). However, the authors did not develop the method further. This idea later received more attention with the concept of self-optimizing control (Skogestad, 2000), where the goal was to find a simple control structure with near-optimal cost, subject to constraints. If the optimal operation occurs when one or more constraints are active, then optimal operation can be achieved by using the available degrees of freedom to tightly regulate the active constraints at its limit (Active constraint control). To illustrate this, consider a oil and gas production system with the following steady-state optimization problem,

$$\begin{aligned} &\min_{\mathbf{u}} \ J(\mathbf{u},\mathbf{d}) \\ &\text{s.t.} \\ &\quad \mathbf{g}(\mathbf{u},\mathbf{d}) \leq 0 \end{aligned} \tag{1}$$

where $\mathbf{u} \in \mathbb{R}^{n_u}$ is the set of manipulated variables (MV) and $\mathbf{d} \in \mathbb{R}^{n_d}$ is the set of disturbances. The cost function is denoted by $J : \mathbb{R}^{n_u} \times \mathbb{R}^{n_d} \rightarrow \mathbb{R}$ and $\mathbf{g} : \mathbb{R}^{n_u} \times \mathbb{R}^{n_d} \rightarrow \mathbb{R}^{n_g}$ denotes the list of constraints. For a given set of disturbances, let $n_a \leq n_g$ denote the number of active constraints $\mathbf{g}_{\mathbb{A}}(\mathbf{u},\mathbf{d})$, then n_a manipulated variables (MV) are used to control n_a controlled variables (CV). In this case, the CV is usually the constraint itself, i.e. CV = $\mathbf{g}_{\mathbb{A}}$. In fact, the case example studied by Morari et al. (1980) to demonstrate the idea of feedback optimizing control resulted in active constraint control. The simplest approach is then to control the active constraints tightly using a simple feedback controller which does not require a detailed model. If a constraint on an MV is active, then we do not even need a controller, since the MV can be simply kept constant at its limit.

2.2. Self-optimizing control for unconstrained MVs

If there are remaining unconstrained degrees of freedom, then so-called "self-optimizing" control variables (CV) should be identified, which when kept at a constant setpoint, gives acceptable loss. The choice of self-optimizing variables is not obvious, and there may be many candidates with similar performance. We need a good model offline in order to identify good self-optimizing variables. One approach is to select an optimal linear combination of measurements as the self-optimizing CV (Halvorsen, Skogestad, Morud, & Alstad, 2003). Not considering measurement noise (error), the ideal self-optimizing CV is the gradient of the cost function with respect to the control input (Skogestad, 2000), i.e. CV = $\mathbf{J_u}$, which when kept at a constant setpoint of zero, satisfies the necessary conditions of optimality (Krishnamoorthy & Skogestad, 2019). Since the gradient is not usually a measured quantity, we need to estimate the steady state cost gradient. One way to estimate the cost gradient is to use a dynamic model of the system as described by Krishnamoorthy, Jahanshahi, and Skogestad (2019a). If a direct cost measurement is available, the cost gradient can also be directly estimated using the cost measurements as done in methods such as extremum seeking control (Krstić & Wang, 2000), NCO-tracking (François, Srinivasan, & Bonvin, 2005) etc. The different approaches to estimate the cost gradient are summarized in Srinivasan, François, and Bonvin (2011).

2.3. Switching between different operating regions

In many cases, the set of active constraints change with different operating conditions. A different set of active constraints requires reconfiguration of the control loops. In most cases, simple logic blocks such as selectors and split-range can be used to easily handle the changes in active constraint regions. The systematic approach to choosing the right logic block is briefly summarized below (Krishnamoorthy & Skogestad, 2019; Reyes-Lúa, Zotică, Skogestad et al., 2018):

1. **CV–CV switching**: When we have one manipulated variable (MV) controlling two or more candidate controlled variables (CV), then selector blocks can be used to choose between the different CVs. For example, a minimum selector block can be used to select the minimum of the two MV values proposed by the two controllers controlling the two CVs. For more detailed information on the pairing rules for CV–CV switching, the reader is referred to Krishnamoorthy and Skogestad (2019).
2. **MV–MV switching**: When we have more than two candidate MV controlling the same CV, then split-range logic can be used to switch between the different MVs as described in Reyes-Lúa, Zotică, Das et al. (2018). Alternatively, valve position controllers or two-setpoint controllers can also be used to switch between two candidate MVs (Reyes-Lúa, Zotică, Skogestad et al., 2018).
3. **CV–MV switching**: When we want to switch between two active constraints, where switching is between a MV and CV constraint, then one should use the rule of pairing this CV and MV (Krishnamoorthy & Skogestad, 2019; Reyes-Lúa, Zotică, Das et al., 2018). By doing so, we do not need any additional logic blocks to switch between these constraints. When the MV constraint becomes active, the MV automatically saturates and the CV constraint is given up. If this rule is not followed, then split-range logic will be required to re-pair the MV and CV.

In summary, by applying the concepts of active constraint control for constrained variables, self-optimizing control for unconstrained degrees of freedom, and logics to switch between the different active constraint regions, we can achieve optimal operation using simple feedback controllers.

3. Case study 1: Gas-lift optimization

In some wells, when the reservoir pressure is not sufficient to lift the fluids to the surface, artificial lift methods are employed to boost the production. One commonly used artificial left method is known as gas-lift, where compressed gas is injected into the well tubing via the well annulus in order to reduce the fluid density. This reduces the hydrostatic pressure drop, hence increasing the flow from the reservoir. However, injecting too much gas causes the frictional pressure drop to increase, which has an opposite effect on the flow rate. At one point, the negative effect of the frictional pressure drop surpasses the effect of the positive hydrostatic pressure drop and the flow from the reservoir starts to decrease. Therefore, there is an optimum gas-lift injection rate that corresponds to maximizing oil production. In addition, if the total amount of the gas that is available for lifting is limited, then this must be optimally allocated among the different wells. The optimal allocation of lift gas may also be constrained by the topside gas processing capacity.

A gas-lifted production network with n_w wells connected to a riser, as shown in Fig. 1, has $2n_w$+1 degrees of freedom, namely, n_w gas-lift injection rates, n_w production valves on the wells and 1 valve on the riser. Typically, the gas-lifted wells are controlled by the gas-lift injection rate only. The production valves on the wells and the riser are kept at its maximum limit (which is either constrained by the physical opening or other effects such as casing–heading etc.), since decreasing the valve position reduces the flow from the reservoir. Thus the production valves are all kept at a constant opening and only n_w gas-lift injection rates

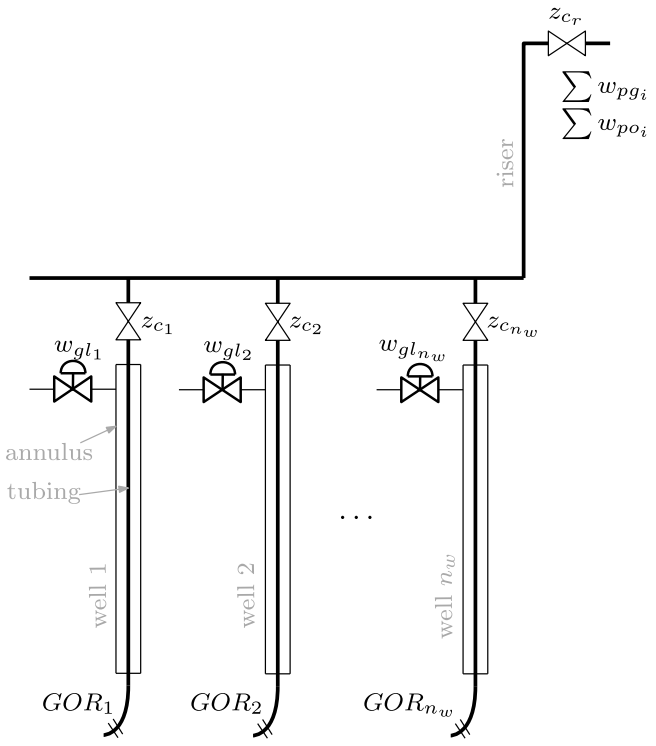

Fig. 1. Schematic representation of a gas-lifted well network.

are the degrees of freedom in this work (Krishnamoorthy, Jahanshahi, & Skogestad, 2018b).

In this section, we show how we can achieve optimal operation of a gas-lifted well network using simple feedback control structures. We consider a production network with n_w gas-lifted wells, producing to a common processing facility. The optimization problem can be stated as:

$$\begin{aligned} \min_{w_{gl_i}} \quad & J = -\$_o \sum_{i=1}^{n_w} w_{po_i} + \$_{gl} \sum_{i=1}^{n_w} w_{gl_i} \\ \text{s.t.} \quad & \sum_{i=1}^{n_w} w_{pg_i} \le w_{pg}^{max} \\ & \sum_{i=1}^{n_w} w_{gl_i} \le w_{gl}^{max} \end{aligned} \tag{2}$$

where $\$_o$ and $\$_{gl}$ are the oil price and the cost of gas compression respectively. w_{po_i} is the produced oil from well i and w_{pg_i} is the produced gas from well i. The gas-lift rate is denoted by w_{gl_i}, which are the manipulated variables. w_{pg}^{max} and w_{gl}^{max} are the maximum gas processing capacity and the maximum gas available for gas-lift respectively (see Fig. 1).

3.1. Control structure design

3.1.1. Unconstrained case

In the unconstrained case, the ideal self-optimizing variable would be the cost gradient with respect to the inputs, which must be equal to zero at the optimum. From (2), this would be given by the expression,

$$\frac{\partial J}{\partial w_{gl_i}} = -\$_o \frac{\partial w_{po_i}}{\partial w_{gl_i}} + \$_{gl} = 0 \quad \forall i \in 1, \dots, n_w \tag{3}$$

In order to achieve the necessary condition of optimality, rearranging (3) gives,

$$\frac{\partial w_{po_i}}{\partial w_{gl_i}} = \frac{\$_{gl}}{\$_o} \quad \forall i \in 1, \dots, n_w \tag{4}$$

The term $\frac{\partial w_{po_i}}{\partial w_{gl_i}}$ is commonly known as *marginal gaslift–oil-ratio* (often abbreviated as marginal GOR), which is defined as the change in oil rate per unit change in the gas-lift injection rate. In the rest of the paper, we denote marginal GOR by

$$\nu_i := \frac{\partial w_{po_i}}{\partial w_{gl_i}}$$

Therefore, in the unconstrained case, the marginal GOR for all the wells ν_i must be controlled to constant setpoint of $\frac{\$_{gl}}{\$_o}$ (Krishnamoorthy et al., 2018b). That is, the controlled variables are

$$CV_1 := \nu_1 \tag{5}$$

controlled to a constant setpoint of $\frac{\$_{gl}}{\$_o}$ and

$$CV_i := (\nu_{i-1} - \nu_i) \quad \forall i = 2, \dots, n_w \tag{6}$$

controlled to a constant setpoint of zero.

3.1.2. Produced gas capacity constraint active

If the total gas processing capacity is low, then the optimum occurs when all the available gas processing capacity is fully utilized. Hence the total gas processing capacity constraint becomes active. We use one well to control this active constraint tightly. For the remaining $(n_w - 1)$ well's gas-lift, the optimum happens when the marginal GOR is equal for all the wells. This is because, for any parallel unit, the optimum happens when the marginal cost is equal as proved in Downs and Skogestad (2011). This concept has been used in gas-lift optimization in several works such as Kanu, Mach, Brown, et al. (1981), Krishnamoorthy et al. (2018b), Sharma and Glemmestad (2013) and Urbanczyk, Wattenbarger, et al. (1994) to name a few.

When it comes to selecting which well to use to control the active constraint tightly, the well with the largest MV (flow) should be used to control the active constraint. This gives better control of the active constraint. Controlling the active constraint with a small MV may quickly saturate, leading to constraint violation or suboptimal operation. In this paper, we assume that the wells are numbered in decreasing order in terms of the flow, with well 1 having the largest flow. Therefore, well 1 is used to control the active constraint.

In this case, the $(n_w - 1)$ self-optimizing CVs are given by,

$$CV_i := (\nu_{i-1} - \nu_i), \quad \forall i = 2, \dots, n_w \tag{7}$$

which are controlled to a constant setpoint of zero, thereby achieving equal marginal GOR. We note that (7) is the same as (6). For well 1, the controlled variable is given by

$$CV_1 := \sum_{i=1}^{n_w} w_{pg_i} \tag{8}$$

which is controlled at its maximum limit of w_{pg}^{max}, thereby achieving active constraint control.

3.1.3. Gas-lift constraint active

When the total available gas-lift is limited such that each of the wells cannot be operated at its local optimum, then the optimum occurs when all the available gas is used for gas-lift. Therefore the total gas-lift constraint is active and one of the well's gas-lift (or more precisely, one degree of freedom related to gas-lift) must be used to control the total gas-lift rate at its maximum limit of w_{gl}^{max}. Again we use the well with the largest MV (flow) for active constraint control as mentioned in Section 3.1.2. For the remaining $(n_w - 1)$ well's gas-lift rate, the optimum happens when the marginal GOR is equal. Therefore, in this case, the $(n_w - 1)$ self-optimizing CVs are given by (7). For active constraint control, the total gas-lift rate must be at its constraint. So,

$$CV_1 := \sum_{i=1}^{n_w} w_{gl_i} \tag{9}$$

which should be controlled to a constant setpoint of w_{gl}^{max}. This may be viewed as an MV constraint, because we can simply keep MV_1 at a constant value of $w_{gl_1} = w_{gl}^{max} - \sum_{i=2}^{n_w} w_{gl_i}$.

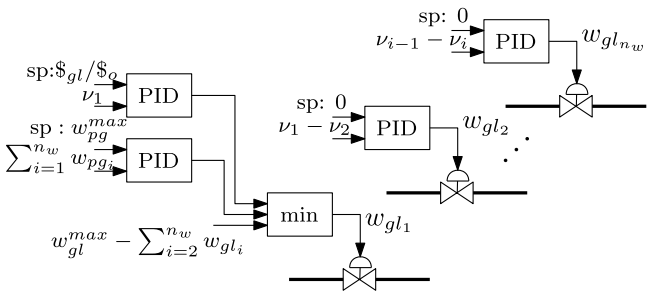

Fig. 2. Schematic representation of the proposed control structure design for optimal operation of a gas-lifted well network.

3.1.4. Summary of cases

A comparison of the three cases shows that, in all the cases, we must control $(n_w - 1)$ self-optimizing CVs given by (7), whereas CV_1 changes:

Case 3.1.1: $CV_1 = \nu_1$ with $CV_1^{sp} = \frac{\$_{gl}}{\$_o}$

Case 3.1.2: $CV_1 = \sum_{i=1}^{n_w} w_{pg_i}$ with $CV_1^{sp} = w_{pg}^{max}$

Case 3.1.3: $CV_1 = \sum_{i=1}^{n_w} w_{gl_i}$ with $CV_1^{sp} = w_{gl}^{max}$

Thus, with the chosen pairings, the CV only changes for well 1 depending on the three operating regions. Since this is a CV–CV switching, we use a minimum selector block to select between (5), (8) and (9). The proposed control structure is schematically represented in Fig. 2.

3.2. Simulation results

In this simulation study, we consider a network of $n_w = 6$, as such we have 6 MVs. For the last 5 MVs, we control the CVs (7) to a constant setpoint of zero, thereby ensuring equal marginal GOR for all the wells. For the first well, we design three controllers to control (5), (8) and (9) and use a minimum selector block to select between the three controllers as shown in Fig. 2. Simple PI controllers are used for all the controllers and the controller gains were tuned using SIMC rules (Skogestad, 2003). The controller tuning parameters are shown in Table 1. For this simulation case example, the model is the same as the one used in Krishnamoorthy, Foss, and Skogestad (2018), but with six wells instead of two wells. The model parameters are shown in Table A.5. The well system is modeled in `MATLAB 2018b` using the `CasADi` toolbox (Andersson, Gillis, Horn, Rawlings, & Diehl, 2018) and the simulator uses `IDAS` integrator.

We use the following data: The ratio of the oil price to cost of compression $\frac{\$_{gl}}{\$_o} = 0.25$. The total available gas-lift is limited to $w_{gl}^{max} = 10$ kg/s and the nominal gas processing capacity is constrained at $w_{pg}^{max} = 30$ kg/s. The production network is simulated for a total of 10 h. As mentioned in Section 2, there are different methods to estimate the steady-state gradient, which is the marginal GOR in this case. In this paper, the marginal GOR is estimated using a nonlinear process model and measurements as described in Krishnamoorthy et al. (2018b, 2019a).

Initially, we assume that the GOR of the different wells are such that the optimum occurs when all the available gas is used for gas-lift and we see that proposed control structure design achieves this

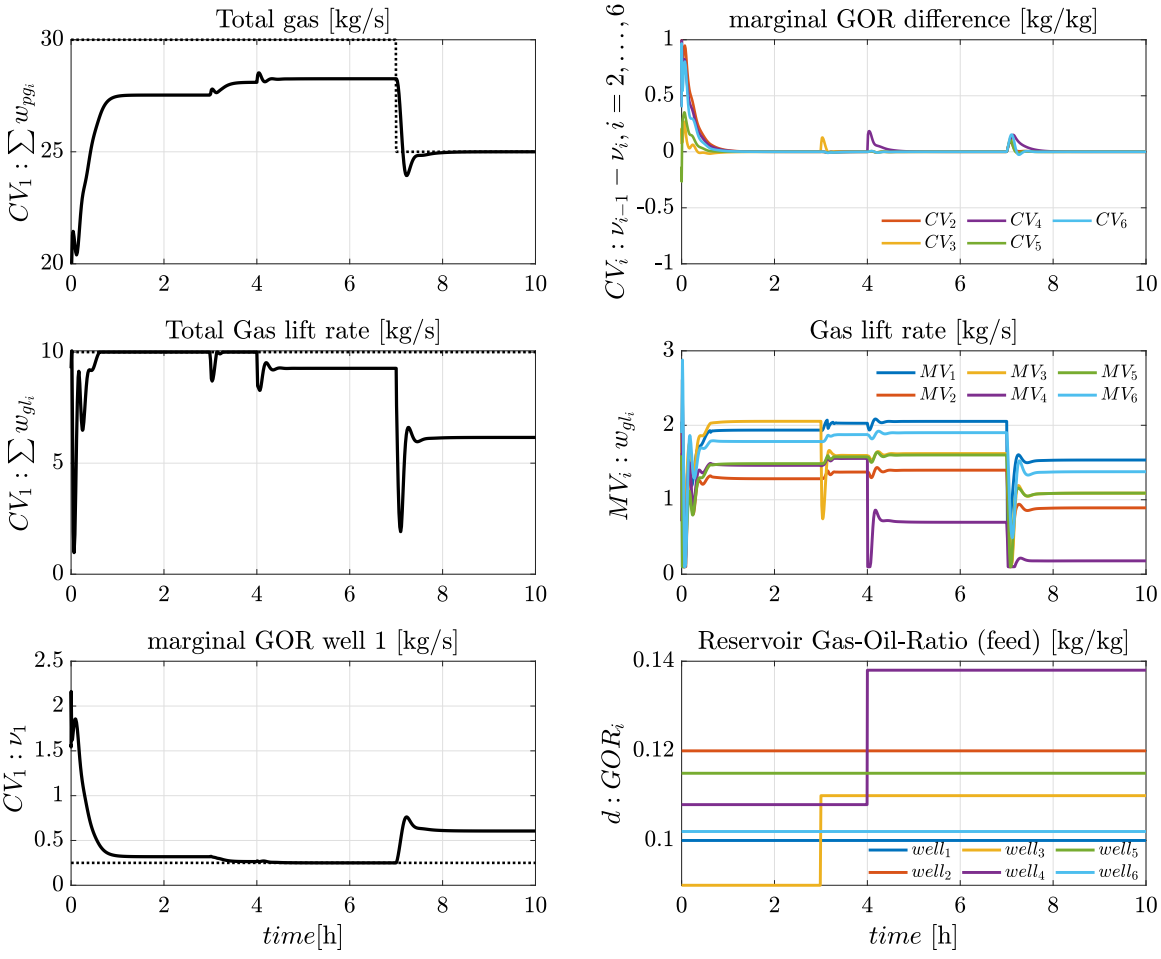

Fig. 3. Case Study 1: Simulation results showing the optimal operation of a production network with 6 gas-lifted wells for varying operating conditions.

Table 1
Controller parameters used in the gas-lift case study.

Well	CV	CV^{sp}	K_P	K_I
Well 2	$v_2 - v_1$	0	13.79	0.0173
Well 3	$v_2 - v_1$	0	9.12	0.0114
Well 4	$v_2 - v_1$	0	13	0.016
Well 5	$v_2 - v_1$	0	12.5	0.015
Well 6	$v_2 - v_1$	0	7.07	0.0089
Well 1	$\sum w_{pg_i}$	w_{tg}^{max}	0.267	3.3e−4
	v_1	$\$_{gl}/\$_o$	9.302	0.0116
	$\sum w_{gl_i}$	w_{gl}^{max}	–	–[a]

[a] No controller is needed for the maximum gas-lift rate $\sum w_{gl_i}$. This is achieved by having a constant MV $w_{gl_1} = w_{gl}^{max} - \sum_{i=2}^{n_w} w_{gl_i}$

by automatically selecting (9) as CV_1. The difference in the marginal GOR for the wells is also controlled to zero, implying that the wells are operated at equal marginal GOR, as shown in Fig. 3. At time $t = 3$ h, a disturbance causes the GOR of well 3 to increase from 0.09 kg/kg to 0.11 kg/kg. The total gas-lift constraint is still active, and the gas-lift injection rates for the different wells are adjusted automatically to optimally allocate the total available gas-lift to reflect the new operating conditions.

At time $t = 4$ h, another disturbance causes the GOR of well 4 to increase from 0.108 kg/kg to 0.138 kg/kg. In this case, neither the total gas-lift constraint nor the gas capacity constraint is active (unconstrained case). When this disturbance happens, the min selector block automatically chooses (5) as CV_1 and we see that the marginal GOR of all the wells are now controlled to a constant value of $\frac{\$_{gl}}{\$_o} = 0.25$.

At time $t = 7$ h, the total topside gas processing capacity reduces from $w_{pg}^{max} = 30$ kg/s to $w_{pg}^{max} = 25$ kg/s. The optimum is then when all the available gas processing capacity is fully utilized. In this case, the min selector automatically switches the CV_1 to (8) and we see that the total gas produced is controlled at its maximum limit of $w_{pg}^{max} = 25$ kg/s. At the same time, the marginal GOR for all wells are kept equal by the proposed controller structure, thus leading to optimal operation for the new operating condition.

From the simulation results, it can be clearly seen that optimal operation under varying operating conditions can be achieved using simple feedback controllers, without the need for advanced optimization tools.

4. Case study 2: ESP lifted well

In the previous section, we used gas lift as the artificial lift technology. Another commonly used technology is to use electric submersible pumps (ESP). ESPs are especially common in heavy oil fields, where the reservoir oil is very viscous and does not flow naturally. ESPs are multistage centrifugal pumps that are placed several meters below inside the well tubing (Takacs, 2017) as depicted in Fig. 4.

The ESP lifted wells are operated by adjusting the rotational speed of the pump (denoted by ω) and the production choke (denoted by z_c), i.e. there are two manipulated variables for each well. Offshore oil fields may have several ESP lifted wells producing to a common manifold, such that the operation of one pump affects the operation of the other ESP lifted wells due to the coupling via the manifold pressure p_m. In addition, the fluid viscosity, reservoir inflow conditions and the available power may also change, which affects the optimal operation.

Traditionally, the operation of an ESP lifted well is decided by the operators together with an external ESP expert team (typically from the ESP vendor). However it may be challenging to operate several ESP lifted wells simultaneously, especially when the wells are highly coupled. It is important to operate the ESP lifted well properly in the presence of disturbances in order to avoid pump failures and to extend the pump life time, since ESP failures can be expensive both in terms of the replacement costs and lost production.

Automatic control of an ESP lifted well can contribute to safe and optimal operation (Pavlov, Krishnamoorthy, Fjalestad, Aske, & Fredriksen, 2014). The objective is to compute the optimal ESP speed and the production choke opening such that the:

- ESP intake pressure is maintained at desired setpoint
- ESP power consumption is minimized
- ESP operation is maintained within a desired operating envelop.

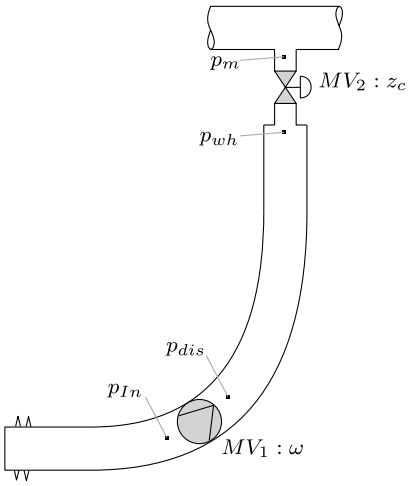

Fig. 4. Schematic representation of an ESP lifted well.

The main objective in controlling an ESP lifted well is to maintain the ESP intake pressure at a desired setpoint, since this gives direct control over the production rate from the reservoir (Krishnamoorthy, Bergheim, Pavlov, Fredriksen and Fjalestad, 2016). In addition, it is desirable to achieve this setpoint using minimal power consumption. For example, this can be achieved by reducing the ESP speed to its minimum limit and manipulate the production choke suitably to achieve the intake pressure setpoint. Reduced ESP frequency directly translates to reduced power consumption, since the power consumed increases cubically with increasing speed, as given by the pump affinity laws (Takacs, 2017),

$$P = P_0 \left(\frac{\omega}{\omega_0} \right)^3 \tag{10}$$

where P_0 is the power consumed at some nominal ESP speed ω_0 and P is the power consumed at frequency ω.

The pump must also be operated within a pre-defined operating envelop, which is constrained by the minimum and maximum ESP speed (ω_{min} and ω_{max}) and two constraints known as upthrust and downthrust limits as shown in Fig. 5. Upthrust and downthrust regions correspond to unbalanced thrust forces either in the upwards or downwards direction, leading to mechanical degradation of the pump. Therefore, it is undesirable to operate in these regions. These are often represented on the pump performance curves, which are usually provided by the ESP vendor. A typical ESP envelope is shown in Fig. 5a as a function of flowrate and pump head. The pump head is given by,

$$H = \frac{(p_{dis} - p_{In})}{\rho g} \tag{11}$$

where p_{In} and p_{dis} are the pump intake and discharge pressures respectively (see Fig. 4) and ρ is the mixture density and g is the acceleration of gravity. In the pump performance curves shown in Fig. 5a, the normal operating envelope is shown by the edges A–B–C–D, where A–B and C–D are the minimum and maximum ESP speed respectively. B–C and A–D are the upthrust and downthrust limits respectively.

The operational envelope in Fig. 5a can be translated to the envelope in Fig. 5b which is plotted as a function of head and ESP speed. Since each line representing the pump characteristics for different frequencies in Fig. 5a, the maximum and minimum head corresponding

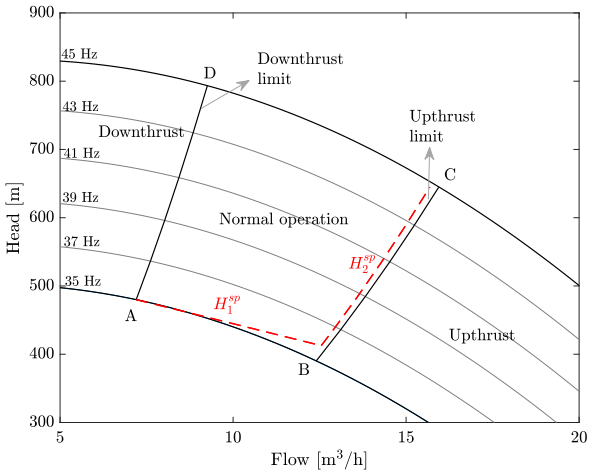

(a)

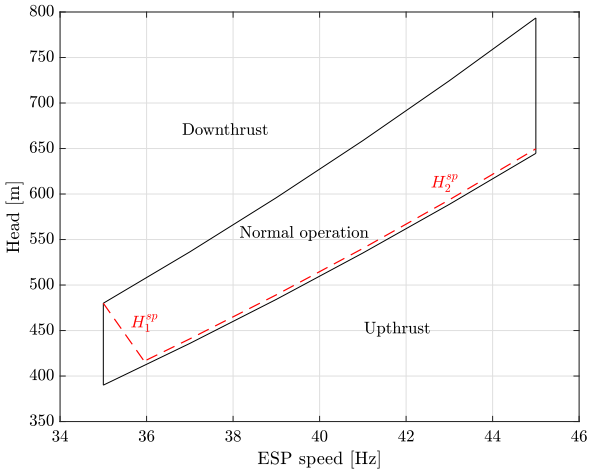

(b)

Fig. 5. ESP operating envelope shown on (a) head versus flow map (b) head versus ESP speed map.

to the upthrust and downthrust limits respectively can be retrieved to translate the envelope in terms of head and ESP speed.[1] The main motivation for translating the pump envelope into head and ESP speed in Fig. 5b is because this envelope is not as sensitive to viscosity unlike the flow vs. head envelope in Fig. 5a. As the water and oil fractions vary, the water and oil mixture forms emulsions, which will lead to significant viscosity changes, especially for heavy oil wells. For most centrifugal pumps, the head is not very sensitive to viscosity up to 500 cP, unlike flow rate, power and pump efficiency. Hence formulating the upthrust and downthrust constraints in terms of head and ESP speed makes it less sensitive to viscosity changes.

4.1. Control structure design

In order to achieve these objectives, optimizing controllers such as model predictive control (MPC) have been proposed in Krishnamoorthy, Bergheim et al. (2016) and Pavlov et al. (2014). In this paper, we show how simple feedback controllers can be used to achieve the same objective.

[1] Note that upthrust corresponds to low head and downthrust corresponds to high head in Fig. 4.

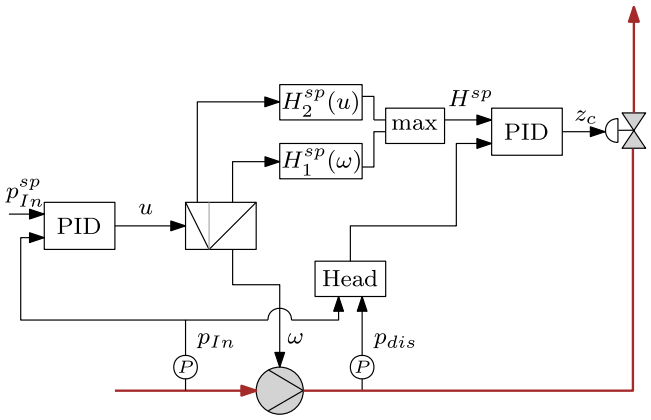

Fig. 6. Proposed control structure design for optimal operation of an ESP lifted well.

In order to reduce the power consumption, we want to minimize the ESP speed, hence the low limit on the ESP speed in Fig. 5b is potentially an active MV constraint. In the presence of disturbances, the pump operation maybe pushed towards the upthrust operating region. In such cases, the upthrust limit becomes active. To handle these different operating conditions, we use a split range controller to control the intake pressure at its setpoint as shown in Fig. 6. The output of this PID control (with nominal range 0%–100%) enters a split range logic. When the output signal u is below a chosen value u_{SR} (e.g. 50%), the ESP speed is kept close its minimum limit $\omega_{min}+\epsilon$ (e.g. between 35 Hz and 36 Hz) to minimize the power consumption. The well head choke is controlled via a lower layer controller that controls the pump head. The corresponding setpoint for the head H_2^{sp} is given by a linear value from maximum to minimum head for the lowest ESP speed.

$$H_2^{sp}(u) = H_{\omega_{min}}^{dn} - \frac{H_{\omega_{min}}^{dn} - H_{\omega_{min}}^{up}}{u_{SR}} u \tag{12}$$

where, $H_{\omega_{min}}^{dn}$ and $H_{\omega_{min}}^{dn}$ are the downthrust and upthrust head corresponding to the minimum ESP speed ω_{min} that are obtained from the ESP operating envelope in Fig. 5. The head measurement is computed using the pump intake and discharge pressure as shown in (11). Head reduction in this case will reduce the ESP intake pressure. Therefore, in this case, the ESP speed is kept close to its minimum ω_{min} and the ESP intake pressure is driven to its setpoint using the well head choke z_c indirectly via the head control (12).

When the first control output gets higher than u_{SR}, then the pump speed increases to maintain the ESP intake pressure at its setpoint. In this case, the upthrust constraint becomes active. Therefore, the head is controlled using the well head choke to maintain it at its upthrust limit and the corresponding setpoint is given as the upthrust head, which is a function of the ESP speed,

$$H_1^{sp}(\omega) = c_{up}\omega^2 \tag{13}$$

The head setpoint in this case is designed such that there is a margin to the actual upthrust limit. Here, the head setpoint essentially follows the upthrust limit (plus a user defined margin) as shown in the operating envelope in Fig. 5b. Note that the pump head scales quadratically with ESP speed as given by the pump affinity laws (Takacs, 2017), hence the square term on the ESP speed in (13). In this case, the intake pressure is controlled using the ESP speed and the wellhead choke in used to control the head at its upthrust limit.[2] To automatically switch between the two head setpoints, (12) and (13), we use a maximum selector block $H^{sp} = \max(H_1^{sp}, H_2^{sp})$, as shown in Fig. 6. The operation of the ESP is

[2] Depending on the optimization objective, one may also choose to follow the best efficiency point (BEP) instead of the upthrust limit for increased ESP lifetime instead of increased production.

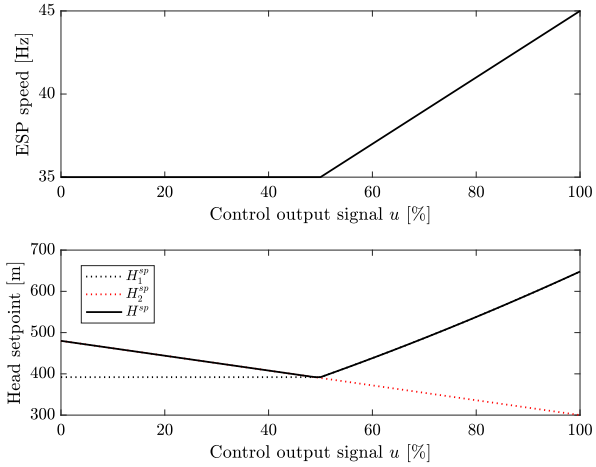

Fig. 7. The ESP speed and the head setpoint as a function of the intake pressure controller output signal.

thus maintained along the red dashed lines that are shown in the ESP envelope in Fig. 5. The ESP speed and the head setpoint as a function of the intake pressure control output u are shown in Fig. 7.

4.2. Experimental results

The proposed control system was tested in a large-scale multi-phase test facility at Equinor research center in Porsgrunn, Norway. The test facility is designed to use live viscous crude oil (crude oil in real well conditions). The ESP installed in the test facility is a full-scale multistage horizontal centrifugal pump with 84 stages. The pump is a 538-P75 SXD model from Baker Hughes and is equipped with a variable speed drive to control the pump speed (Yang, Sannæs, Johnson, Sjøvoll, Schulkes, et al., 2012).

The layout of the multiphase flow loop is shown in Fig. 8. The oil and water stream from the main separator is fed to the ESP with the help of feeder pumps. The heat exchanges allow the fluids to be cooled to a desired temperature. The oil feeder pump and the corresponding split stream are controlled such that the flow rate is inversely proportional to the ESP intake pressure. The water split stream is controlled using a ratio controller to get the desired watercut. As such, the main separator along with the oil and water feed pumps emulate the reservoir inflow in to the well. Water and oil is mixed upstream the ESP and enters the ESP. The fluid mixture is then directed through a 2″ test section that is 200 m long. This section emulates the well tubing. A choke downstream this 2″ test section is used as the production choke as indicated in Fig. 8. The fluid mixture is then redirected back to the main separator. The specifications of the test facility are summarized in Table 2.

The PID controllers, logic blocks and the calculation blocks to compute the head setpoint were all implemented in the process control system from Kongsberg AIM process control system that is normally used for operation of the test facility. Adjustment of setpoints, controller parameters and the signal range are carried out from the same user interface that the operators are familiar with. The PID controllers were tuned using trial and error method and are shown in Table 3.

For the ESP in the test facility, the minimum and maximum ESP speed were 35 Hz and 45 Hz respectively. The split range controller used to control the ESP intake pressure was designed with $u_{SR} = 50\%$, where the ESP speed is kept between 35 Hz and 36 Hz when the controller output is below $u_{SR} = 50\%$ and the head is kept at its upthrust limit when the controller output is above $u_{SR} = 50\%$. The head setpoints were computed according to (13) and (12) for the regions below and above $u_{SR} = 50\%$. The different parameter values used to compute the head setpoints are shown in Table 4.

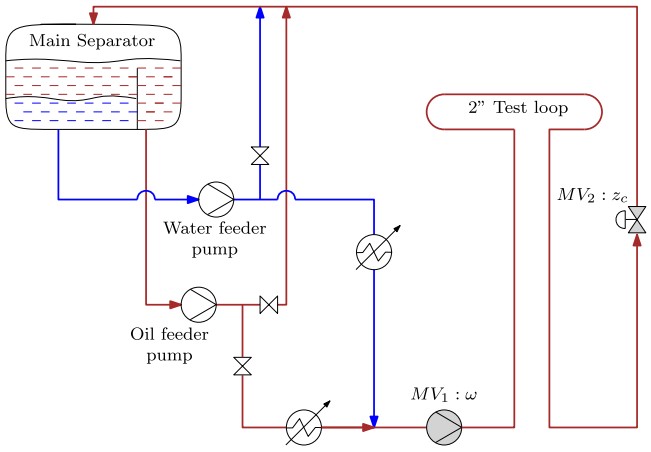

Fig. 8. Schematic representation of the large-scale experimental test facility used to test the proposed control structure.

Table 2
Test facility specifications.

No. of phases	3 (oil, water and gas)
Fluids	Saline water, crude oil, natural gas
Oil flow rate	0–15 m^3/h
Water flow rate	0–10 m^3/h
Liquid flow rate	0–25 m^3/h
Max pressure at ESP	175 bar
Temperature range	4–110 °C
Nominal oil viscosity	70 cP (at ~40 °C)
Pipe internal diameter	0.05248–0.079 m
Total liquid volume	8.3 m^3
Material	Duplix stainless steel 22 Cr

Table 3
Controller tuning parameters used in Fig. 6.

	K_P	K_I
Intake pressure control	1	0.05
Head control	0.05	2.5e−3

Table 4
Parameters used in the control structure design shown in Fig. 6.

Parameter	Value
$H^{dn}_{\omega_{min}}$	480 m
$H^{up}_{\omega_{min}}$	390 m
c_{up}	0.32
u_{SR}	50%

The proposed control structure was tested for a total of 2 h (from 9:00 to 11:00). The experiment starts with 0% watercut. The controllers were turned on at time 09:05 and we see that the intake pressure is driven to its setpoint as shown in Fig. 9. The setpoint for the ESP intake pressure and the head are shown in solid red lines and the measured intake pressure and the head are shown in solid black lines. The upthrust and downthrust constraints are shown in red dotted lines. The ESP speed and the well head choke are also shown in solid black lines and the maximum and minimum MV limits are shown in red dotted lines, as clearly marked in Fig. 9. The ESP head is also plotted on the head Vs. speed envelope which shows that the proposed control structure design is able to maintain the ESP operation inside the safe operating envelope as shown in Fig. 10. It is important to note that when large disturbances such as flow inversion happens, the pump violates the upthrust limit only dynamically, which is acceptable.

At time 09:13, the ESP intake pressure was changed from 39 bar to 37 bar and the new intake pressure setpoint is achieved by the controllers as shown in Fig. 9. It can also be seen that this is achieved

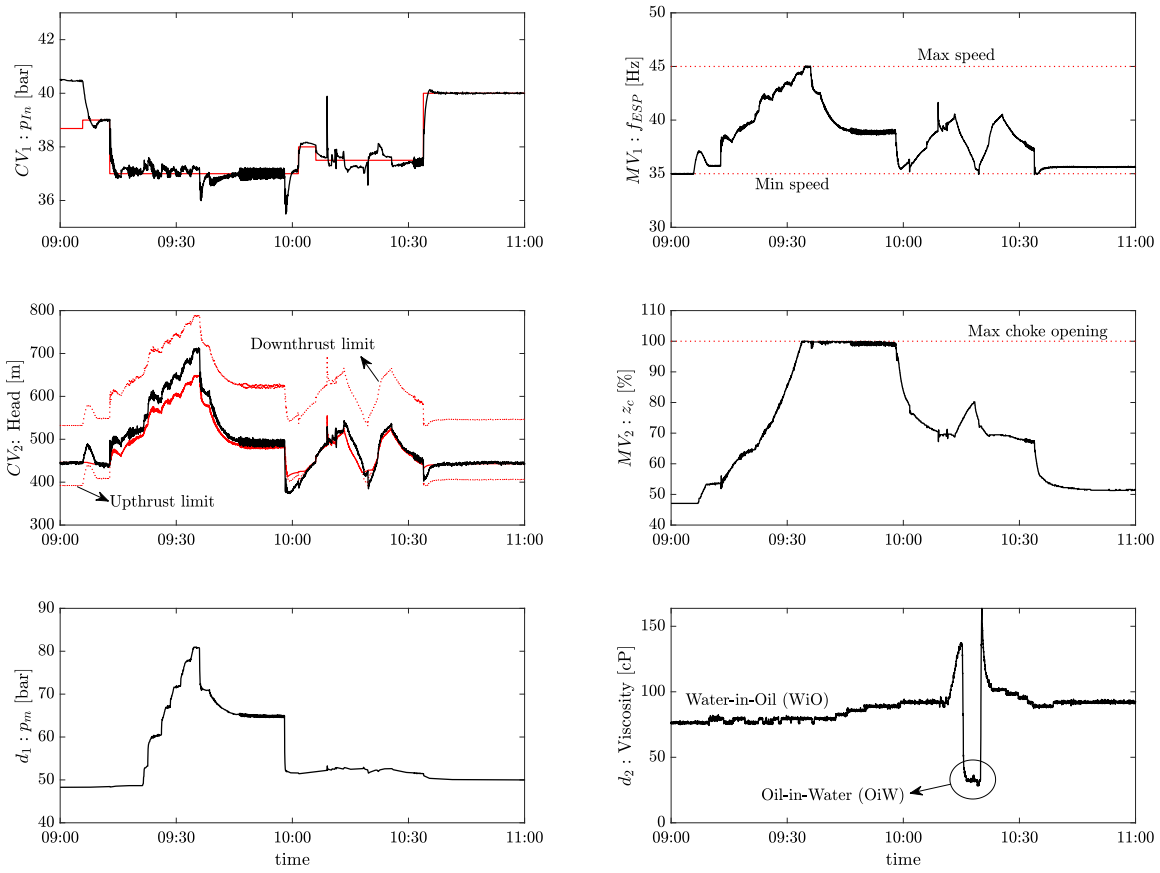

Fig. 9. Case study 2: Experimental results using the proposed control structure. Measured values are shown in solid black lines, setpoints are shown in solid red lines and constraints are shown in red dotted lines. (For interpretation of the references to color in this figure legend, the reader is referred to the web version of this article.)

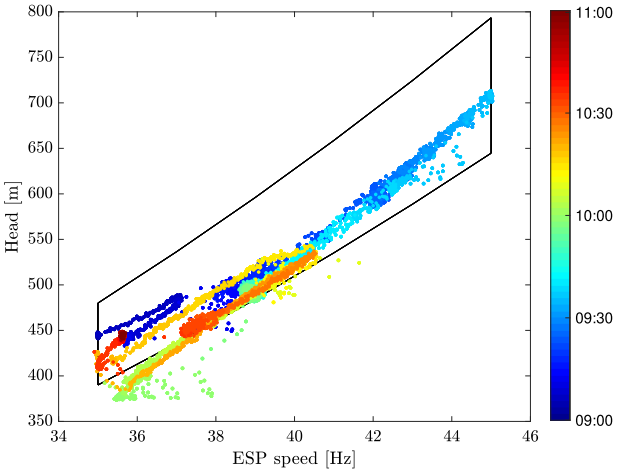

Fig. 10. Experimental results using the proposed control structure. Measured head plotted on the operating envelope. Color bar on the right indicates time.

by keeping the ESP speed close to its minimum (i.e. between 35 Hz and 36 Hz in this case).

As mentioned earlier, one of the most common disturbance to an ESP lifted well is the manifold pressure (due to the coupling between the different wells). To emulate this disturbance, the pressure downstream the production choke was varied between times 09:20 and 09:55 as shown in the bottom-left subplot in Fig. 9. When this disturbance happens, it can be seen that the intake pressure controlled output increases above $u_{SR} = 50\%$ and the ESP speed is increased to maintain the intake pressure setpoint. Consequently, the head setpoint now coincides with the upthrust limit as shown in Fig. 9 and the production choke is increased to follow the head setpoint.

At time 09:45, the watercut starts to increase slowly and consequently, the mixture viscosity starts to increase due to water-in-oil (WiO) emulsion formation. This can be seen in the bottom right subplot in Fig. 9. As the watercut increases, the ESP speed increases to maintain the intake pressure at its setpoint and the head setpoint coincides with the upthrust limit. At 10:15, the watercut is high enough to cause an inversion from water-in-oil emulsion[3] to oil-in-water emulsion.[4] When this happens, there is a significant drop in viscosity from ~140cP to ~30cP. At 10:20, the water cut is reduced again and we see that the emulsion inverts back to water-in-oil emulsion. During the flow inversions, there is a significant change in the viscosity and it can be seen that the proposed control structure is able to maintain the intake pressure at its setpoint and maintain the ESP operating within the operating envelop.

Several other tests were conducted at the Equinor test facility to validate the use of simple PID control structures for optimal operation of the ESP lifted well. These lasted over 6 days. The test campaign also involved repeating the tests several times to ensure repeatability and reproducibility of the test results. The overall conclusion from the test campaign was that PID controllers were able to consistently achieve the control objectives and simple logics such as split range and selectors were sufficient to handle changes in different operating regions. For the sake of brevity, only a few test points are presented in this paper. Based on the test results, the use of automatic control of ESP lifted wells were qualified for first-use in Equinor operated fields.

[3] Water droplets suspended in oil medium.
[4] Oil droplets suspended in water medium.

Table A.5
Model parameters used in the gas lift well model equations from Krishnamoorthy et al. (2018).

Parameter	Description	Unit	Well 1	Well 2	Well 3	Well 4	Well 5	Well 6	Riser
L_w	Length of well tubing	[m]	1500	1500	1500	1500	1500	1500	–
H_w	Height of well tubing	[m]	1000	1000	1000	1000	1000	1000	–
D_w	Diameter of well tubing	[m]	0.121	0.121	0.121	0.121	0.121	0.121	–
L_{bh}	Length of well below injection	[m]	500	500	500	500	500	500	–
H_{bh}	Height of well below injection	[m]	500	500	500	500	500	500	–
D_{bh}	Diameter of well below injection	[m]	0.121	0.121	0.121	0.121	0.121	0.121	–
L_a	Length of well annulus	[m]	1500	1500	1500	1500	1500	1500	–
H_a	Height of well annulus	[m]	1000	1000	1000	1000	1000	1000	–
D_a	Diameter of well annulus	[m]	0.189	0.189	0.189	0.189	0.189	0.189	–
L_r	Length of riser	[m]	–	–	–	–	–	–	500
H_r	Height of riser	[m]	–	–	–	–	–	–	500
D_r	Diameter of riser	[m]	–	–	–	–	–	–	0.121
ρ_o	Oil density	[kg/m^3]	800	800	790	800	820	805	–
GOR_0	Nominal gas–oil-ratio	[kg/kg]	0.1	0.12	0.09	0.108	0.115	0.102	–
p_{res}	Reservoir pressure	[bar]	150	155	155	160	155	155	–
PI	Productivity index	[kg/s/bar]	7	7	7	7	7	7	–
C_iv	Injection valve characteristics	[m^2]	0.1E−3	0.1E−3	0.1E−3	0.1E−3	0.1E−3	0.1E−3	–
C_pc	Production valve characteristics	[m^2]	2E−3	2E−3	2E−3	2E−3	2E−3	2E−3	–
C_pr	Riser valve characteristics	[m^2]	10E−3	10E−3	10E−3	10E−3	10E−3	10E−3	–
T_a	Annulus temperature	[°C]	28	28	28	28	28	28	–
T_w	Well tubing temperature	[°C]	32	32	32	32	32	32	–
T_r	Riser temperature	[°C]	–	–	–	–	–	–	30
M_w	Molecular weight of gas	[g]	20	20	20	20	20	20	20

5. Conclusion

Using a simulation case study and an experimental study, we showed that simple PID controller structures are sufficient to achieve optimal operation of oil and gas production systems under different operating conditions. The main advantage of using conventional PID control structure is that they are easy to implement, tune and maintain. These are well known tools that have been in use in the offshore oil and gas industry for decades. With simple control structures, we avoid most of the technological and people-related challenges mentioned in Section 1. Consequently, there is a higher chance of adopting such optimal control tools, irrespective of the corporate culture.

This was also observed during our experimental study at the Equinor test facility where the operators felt comfortable using the controllers after a short introduction to the features. The operators also reported reduced workload while operating the test facility with the controllers and some of the controllers were also used by the operators even after the experimental study was concluded.

Declaration of competing interest

None declared.

Acknowledgments and author contribution

DK developed and designed the gas lifted well models and carried out the simulation study under the supervision of SS. DK and KF were involved in the development, testing and validation of simple control structures for ESP control at the Equinor test facility in Porsgrunn. DK prepared the manuscript. SS and KF contributed to reviewing and correcting the manuscript.

The authors would like to thank Equinor ASA for the opportunity to publish the ESP control test campaign. DK and KF would like to thank the ESP automation team at Equinor research center, which includes Alexey Pavlov (now with NTNU), Elvira M. Bergheim and Morten Fredriksen, for useful and interesting discussions during the test campaign. DK and KF would also like to thank all the operators at the Equinor test facility. DK and SS also gratefully acknowledge the financial support from SFI SUBPRO, which is financed by the Research Council of Norway, major industry partners and NTNU.

Appendix - Gas lifted well network model

Production from a cluster of $\mathcal{N} = \{1, \dots, n_w\}$ gas lifted well can be described using differential and algebraic equations (Krishnamoorthy, Foss and Skogestad, 2016; Krishnamoorthy, Foss, & Skogestad, 2017). The dynamics are include in the model due to the mass balances in each well which are described by the following differential equations.

$$\dot{m}_{ga_i} = w_{gl_i} - w_{iv_i} \tag{A.1a}$$

$$\dot{m}_{gt_i} = w_{iv_i} - w_{pg_i} + w_{rg_i} \tag{A.1b}$$

$$\dot{m}_{ot_i} = w_{ro_i} - w_{po_i} \qquad \forall i \in \mathcal{N} \tag{A.1c}$$

where, m_{ga_i} is the mass of gas in the annulus, m_{gt_i} is the mass of gas in the well tubing, m_{ot_i} is the mass of oil in the well tubing, w_{gl_i} is the gas lift injection rate, w_{iv_i} is the gas flow from the annulus into the tubing, w_{pg_i} and w_{po_i} are the produced gas and oil flow rates respectively and, w_{rg_i} and w_{ro_i} are the gas and oil flow rates from the reservoir for each well i. The mass balance in the riser for oil and gas phase is given by,

$$\dot{m}_{gr} = \sum_{i=1}^{n_w} w_{pg_i} - w_{tg} \tag{A.2a}$$

$$\dot{m}_{or} = \sum_{i=1}^{n_w} w_{po_i} - w_{to} \tag{A.2b}$$

where, m_{gr} is the mass of gas in the riser and m_{or} is the mass of oil in the riser and w_{tg} and w_{to} are the total gas and oil flow rates respectively. The densities ρ_{a_i} (density of gas in the annulus in each well) and ρ_{m_i} (fluid mixture density in the tubing for each well) and ρ_r (fluid mixture density in the riser) are given by,

$$\rho_{a_i} = \frac{M_w p_{a_i}}{T_{a_i} R} \tag{A.3a}$$

$$\rho_{w_i} = \frac{m_{gt_i} + m_{ot_i} - \rho_o L_{bh_i} A_{bh_i}}{L_{w_i} A_{w_i}} \tag{A.3b}$$

$$\rho_r = \frac{m_{gr} + m_{or}}{L_r A_r} \qquad \forall i \in \mathcal{N} \tag{A.3c}$$

where M_w is the molecular weight of the gas, R is the gas constant, T_{a_i} is the temperature in the annulus in each well, ρ_o is the density of oil in the reservoir, L_{bh_i} and L_{w_i} are the lengths of each well above and below the injection point respectively and A_{bh_i} and A_{w_i} are the cross-sectional area of each well above and below the injection point respectively. L_r and A_r are the length and the cross sectional area of

the riser manifold. The annulus pressure p_{a_i}, wellhead pressure p_{wh_i}, well injection point pressure w_{iv_i} and the bottom hole pressure p_{bh_i} for each well are given by,

$$p_{a_i} = \left(\frac{T_{a_i}R}{V_{a_i}M_w} + \frac{gH_{a_i}}{L_{a_i}A_{a_i}}\right)m_{ga_i} \tag{A.4a}$$

$$p_{wh_i} = \frac{T_{w_i}R}{M_w}\left(\frac{m_{gt_i}}{L_{w_i}A_{w_i} + L_{bh_i}A_{bh_i} - \frac{m_{ot_i}}{\rho_o}}\right) \tag{A.4b}$$

$$p_{wi_i} = p_{wh_i} + \frac{g}{L_{w_i}A_{w_i}}(m_{ot_i} + m_{gt_i} - \rho_o L_{bh_i}A_{bh_i})H_{w_i} + \Delta p_{fric} \tag{A.4c}$$

$$p_{bh_i} = p_{wi_i} + \rho_{w_i} g H_{bh_i} + \Delta p_{fric} \qquad \forall i \in \mathcal{N} \tag{A.4d}$$

where L_{a_i} and A_{a_i} are the length and cross sectional area of each annulus, T_{w_i} is the temperature in each well tubing, H_{r_i} and H_{w_i} are the vertical height of each well tubing below and above the injection point respectively and g is the acceleration of gravity constant. The manifold pressure p_m and the riser head pressure p_{rh} are given by,

$$p_{rh} = \frac{T_r R}{M_w}\left(\frac{m_{gr}}{L_r A_r}\right) \tag{A.5a}$$

$$p_m = p_{rh} + \rho_r g H_r + \Delta p_{fric} \tag{A.5b}$$

where T_r is the average temperature in the riser and H_r is the vertical height of the riser. The flow through the downhole gas lift injection valve w_{iv_i}, total flow through the production choke w_{pc_i}, produced gas and oil flow rate, and the reservoir oil and gas flow rates are given by,

$$w_{iv_i} = C_{iv_i}\sqrt{max(0, \rho_{a_i}(p_{a_i} - p_{wi_i}))} \tag{A.6a}$$

$$w_{pc_i} = C_{pc_i}\sqrt{max(0, \rho_{w_i}(p_{wh_i} - p_m))} \tag{A.6b}$$

$$w_{pg_i} = \frac{m_{gt_i}}{m_{gt_i} + m_{ot_i}} w_{pc_i} \tag{A.6c}$$

$$w_{po_i} = \frac{m_{ot_i}}{m_{gt_i} + m_{ot_i}} w_{pc_i} \tag{A.6d}$$

$$w_{ro_i} = PI_i(p_{r_i} - p_{bh_i}) \tag{A.6e}$$

$$w_{rg_i} = GOR_i \cdot w_{ro_i} \qquad \forall i \in \mathcal{N} \tag{A.6f}$$

where, C_{iv_i} and C_{pc_i} are the valve flow coefficients for the downhole injection valve and the production choke for each well respectively, PI_i is the reservoir productivity index, p_{r_i} is the reservoir pressure and GOR_i is the gas–oil ratio for each well. The two wells produce to a common manifold, where the manifold pressure is denoted by p_m and the flow rates from the two well mixes together. The total flow through the riser head choke w_{rh}, the total produced oil and gas rates are then given by,

$$w_{rh} = C_{rh}\sqrt{\rho_r(p_{rh} - p_s)} \tag{A.7a}$$

$$w_{tg} = \frac{m_{gr}}{m_{gr} + m_{or}} w_{rh} \tag{A.7b}$$

$$w_{to} = \frac{m_{or}}{m_{gr} + m_{or}} w_{rh} \tag{A.7c}$$

where C_{rh} is the valve flow coefficient for the riser head valve and p_s is the separator pressure, which is assumed to be held at a constant value.

As seen from (A.1a)–(A.7c), the gas lifted well is modeled as a semi-explicit index-1 DAE system of the form

$$\dot{x} = f(x, z, u, p) \tag{A.8a}$$

$$g(x, z, u, p) = 0 \tag{A.8b}$$

where $f(x, z, u)$ is the set of differential equations (A.1a)–(A.2b) and $g(x, z, u)$ is the set of algebraic equations (A.3a)–(A.7c).

It is worth noting that the process model present above was compared with high fidelity dynamic simulators such as OLGA in Codas, Jahanshahi, and Foss (2016) which ensures that the models used are representative of the real system.

References

Andersson, J. A. E., Gillis, J., Horn, G., Rawlings, J. B., & Diehl, M. (2018). CasADi – A software framework for nonlinear optimization and optimal control. *Mathematical Programming Computation*.

Bieker, H. P., Slupphaug, O., Johansen, T. A., et al. (2007). Real-time production optimization of oil and gas production systems: A technology survey. *SPE Production & Operations*, *22*(04), 382–391.

Binder, B. J. T., Kufoalor, D. K. M., Pavlov, A., & Johansen, T. A. (2014). Embedded model predictive control for an electric submersible pump on a programmable logic controller. In *Control applications (CCA), 2014 IEEE conference on* (pp. 579–585). IEEE.

Campos, M., Teixeira, H., Liporace, F., & Gomes, M. (2009). Challenges and problems with advanced control and optimization technologies. *IFAC Proceedings Volumes*, *42*(11), 1–8.

Codas, A., Jahanshahi, E., & Foss, B. (2016). A two-layer structure for stabilization and optimization of an oil gathering network. *IFAC-PapersOnLine (DYCOPS)*, *49*(7), 931–936.

Darby, M. L., Nikolaou, M., Jones, J., & Nicholson, D. (2011). RTO: An overview and assessment of current practice. *Journal of Process Control*, *21*(6), 874–884.

Downs, J. J., & Skogestad, S. (2011). An industrial and academic perspective on plantwide control. *Annual Reviews in Control*, *35*(1), 99–110. http://dx.doi.org/10.1016/j.arcontrol.2011.03.006.

Forbes, M. G., Patwardhan, R. S., Hamadah, H., & Gopaluni, R. B. (2015). Model predictive control in industry: Challenges and opportunities. *IFAC-PapersOnLine*, *48*(8), 531–538.

Foss, B., Knudsen, B. R., & Grimstad, B. (2018). Petroleum production optimization–a static or dynamic problem? *Computers & Chemical Engineering*, *114*, 245–253.

François, G., Srinivasan, B., & Bonvin, D. (2005). Use of measurements for enforcing the necessary conditions of optimality in the presence of constraints and uncertainty. *Journal of Process Control*, *15*(6), 701–712.

Halvorsen, I. J., Skogestad, S., Morud, J. C., & Alstad, V. (2003). Optimal selection of controlled variables. *Industrial and Engineering Chemistry Research*, *42*(14), 3273–3284.

Hedrick, J., Philips, S., Crivello, T., & Sakoclus, K. (2003). Well optimization extends reservoir life. *Hart's E & P*, *76*(5), 65–67.

Kanu, E. P., Mach, J., Brown, K. E., et al. (1981). Economic approach to oil production and gas allocation in continuous gas lift (includes associated papers 10858 and 10865). *Journal of Petroleum Technology*, *33*(10), 1–887.

Krishnamoorthy, D., Bergheim, E. M., Pavlov, A., Fredriksen, M., & Fjalestad, K. (2016). Modelling and robustness analysis of model predictive control for electrical submersible pump lifted heavy oil wells. *IFAC-PapersOnLine (DYCOPS)*, *49*(7), 544–549.

Krishnamoorthy, D., Foss, B., & Skogestad, S. (2016). Real time optimization under uncertainty - applied to gas lifted wells. *Processes*, *4*(4), http://dx.doi.org/10.3390/pr4040052.

Krishnamoorthy, D., Foss, B., & Skogestad, S. (2017). Gas lift optimization under uncertainty. *Computer Aided Chemical Engineering*, *40*, 1753–1758.

Krishnamoorthy, D., Foss, B., & Skogestad, S. (2018). Steady-state real-time optimization using transient measurements. *Computers & Chemical Engineering*, *115*, 34–45.

Krishnamoorthy, D., Jahanshahi, E., & Skogestad, S. (2018b). Gas-lift optimization by controlling marginal gas-oil ratio using transient measurements. *IFAC International Workshop on Automatic Control in Offshore Oil and Gas Production*, *51*(8), 19–24.

Krishnamoorthy, D., Jahanshahi, E., & Skogestad, S. (2019a). A feedback real time optimization strategy using a novel steady-state gradient estimate and transient measurements. *Industrial and Engineering Chemistry Research*, *58*(1), 207–216.

Krishnamoorthy, D., & Skogestad, S. (2019). Online process optimization with active constraint set changes using simple control structures. *Industrial & Engineering Chemistry Research*, *58*(30), 13555–13567. http://dx.doi.org/10.1021/acs.iecr.9b00308.

Krstić, M., & Wang, H.-H. (2000). Stability of extremum seeking feedback for general nonlinear dynamic systems. *Automatica*, *36*(4), 595–601.

Mayne, D. (2015). Robust and stochastic mpc: Are we going in the right direction? *IFAC-PapersOnLine*, *48*(23), 1–8.

Mochizuki, S., Saputelli, L. A., Kabir, C. S., Cramer, R., Lochmann, M. J., Reese, R. D., et al. (2004). Real time optimization: Classification and assessment. In *SPE annual technical conference and exhibition*. Society of Petroleum Engineers.

Morari, M., Arkun, Y., & Stephanopoulos, G. (1980). Studies in the synthesis of control structures for chemical processes: Part i: Formulation of the problem. process decomposition and the classification of the control tasks. analysis of the optimizing control structures. *AIChE Journal*, *26*(2), 220–232.

Palen, W., Goodwin, A., et al. (1996). Increasing production in a mature basin:" the choke model". In *European petroleum conference*. Society of Petroleum Engineers.

Pavlov, A., Krishnamoorthy, D., Fjalestad, K., Aske, E., & Fredriksen, M. (2014). Modelling and model predictive control of oil wells with electric submersible pumps. In *IEEE conference on control applications (CCA)* (pp. 586–592). IEEE.

Qin, S., & Badgwell, T. A. (2003). A survey of industrial model predictive control technology. *Control Engineering Practice*, *11*(7), 733–764.

Reeves, D., Harvey Jr., R., Smith, T., et al. (2003). Gas lift automation: Real time data to desktop for optimizing an offshore gom platform. In *SPE annual technical conference and exhibition*. Society of Petroleum Engineers.

Reyes-Lúa, A., Zotică, C., Das, T., Krishnamoorthy, D., & Skogestad, S. (2018). Changing between active constraint regions for optimal operation: Classical advanced control versus model predictive control. In *Computer aided chemical engineering, Vol. 43* (pp. 1015–1020). Elsevier.

Reyes-Lúa, A., Zotică, C., & Skogestad, S. (2018). Optimal operation with changing active constraint regions using classical advanced control. *IFAC-PapersOnLine*, *51*(18), 440–445.

Sharma, R., & Glemmestad, B. (2013). On generalized reduced gradient method with multi-start and self-optimizing control structure for gas lift allocation optimization. *Journal of Process Control*, *23*(8), 1129–1140.

Skogestad, S. (2000). Plantwide control: The search for the self-optimizing control structure. *Journal of Process Control*, *10*(5), 487–507.

Skogestad, S. (2003). Simple analytic rules for model reduction and PID controller tuning. *Journal of Process Control*, *13*(4), 291–309.

Srinivasan, B., François, G., & Bonvin, D. (2011). Comparison of gradient estimation methods for real-time optimization. In *21st European Symposium on computer aided process engineering-ESCAPE 21* (pp. 607–611). Elsevier, no. EPFL-CONF-155235.

Takacs, G. (2017). *Electrical submersible pumps manual: design, operations, and maintenance*. Gulf professional publishing.

Urbanczyk, C. H., Wattenbarger, R. A., et al. (1994). Optimization of well rates under gas coning conditions. *SPE Advanced Technology Series*, *2*(02), 61–68.

Yang, Z., Sannæs, B. H., Johnson, G. W., Sjøvoll, M., Schulkes, R. M., et al. (2012). Oil/water flow experiments with live viscous crude: The influence of ESP on flow behavior. In *Offshore technology conference*. Offshore Technology Conference.